Neutron decay from the giant resonance via the ^{10}B(e,$e'n$) reaction

H. Ueno, T. Kawamura,* T. Suzuki,† and H. Taneichi
Department of Physics, Yamagata University, Kojirakawa, Yamagata 990-8560, Japan

T. Saito,‡ T. Nakagawa,§ and K. Kino‖
Laboratory of Nuclear Science, Tohoku University, Mikamine, Taihaku-ku, Sendai 982-0826, Japan

T. Nakagawa
Department of Physics, Tohoku University, Aramaki, Aoba-ku, Sendai 980-8578, Japan

Y. Matsuura¶ and M. Higuchi
Faculty of Engineering, Tohoku Gakuin University, Chuo, Tagajo 985-8537, Japan
(Received 27 August 2009; published 16 December 2009)

The cross sections and angular correlations for neutron decay into various states in the residual nucleus following the ^{10}B(e,$e'n$) reaction have been measured over the excitation energy range of 18–33 MeV at an effective momentum transfer of 0.56 fm^{-1}. In the giant resonance, neutron emission leads to the population of two higher excited states in addition to the ground-state transition: 6.97 MeV $7/2^-(n_5)$ and 11.70 MeV $7/2^- + 12.06$ MeV $3/2^-(n_{6,7})$. This is the first observation of the neutron population of these states. The angular correlations for n_0 show a strong forward-backward asymmetry, which suggests interference from a transition with the opposite parity to $E1$. The angular correlations for n_5 and $n_{6,7}$ have a peak shift of about 50° at lower excitation energy and recover above about 24 and 25 MeV for n_5 and $n_{6,7}$, respectively. Their patterns are considerably different from that for n_0. The angular correlations for each transition were fitted with a Legendre polynomial. The longitudinal-transverse interference coefficient C_2/A_0 is negligible for all populations. For n_0 decay, all Legendre coefficients b_i are positive, but b_2 and b_3 for the n_5 and $n_{6,7}$ decays are negative at lower excitation energy, and the latter causes a shift of the forward peak. The negative values may come from the signs of the phase differences of $\cos\delta_{21}$ and $\cos\delta_{20}$. The ^{10}B(e,$e'n$) cross section measured up to $E_x \sim 32$ MeV agrees well with that of ^{10}B(γ,n), except for a peak at 23 MeV of the giant resonance. In comparison with shell-model calculations, the partial cross section for n_0 is sizable up to higher excitation energy, and predicted large partial cross sections populating the 6.97 MeV $7/2^-$ and 11.70 MeV $7/2^- + 12.06$ MeV $3/2^-$ states in the giant resonance were not observed.

DOI: 10.1103/PhysRevC.80.064609 PACS number(s): 25.30.Fj, 24.30.Cz, 27.20.+n

I. INTRODUCTION

The giant resonance region of ^{10}B was investigated using the (γ,n) reaction [1–4]. Ahsan *et al.* [1] observed a split $E1$-giant resonance region with maxima at 20.2 and 23.0 MeV, as in earlier studies [2–4]. They interpreted it as being because of an asymmetry, analogous to the splitting of the giant resonance in deformed nuclei. The observed giant resonance is consistent with shell-model calculations by Gol'tsov and Goncharova [5], but a peak predicted at ≈11 MeV [5] was not observed. However, data for the (γ, p) reaction are few [6,7]. In our previous study [7], the giant resonance for the odd-odd nucleus ^{10}B was investigated using the (e, p) and (e,d_0) reactions. From the ^{10}B(e, p) reaction, the cross sections for (γ, p_0) and (γ, p_2) were obtained separately. However, cross sections for decay protons of the high-lying states in the residual nucleus could not be obtained because of oxygen contamination in the thin boron target. The integrated cross section for the sum of (γ, p_0) and (γ, p_2) cross sections up to 27 MeV is 6.1 ± 0.2 MeV mb, which corresponds to about 4.1 ± 0.2% of the classical sum rule value. However, the integrated cross section for (γ,n) up to 24.5 MeV represents 30% of the classical sum rule value. The small sum rule value for (γ, $p_{0,2}$) may originate from the lack of transition to high-lying states, as predicted by shell-model calculations [5]. In the (e,$e'n$) reaction, a thick target can be used, which keeps the target free from oxygen contamination.

In this article we report measurements of the cross sections and angular correlations for the ^{10}B(e, $e'n$)^{9}B reaction and compare the results with those of the ^{10}B(γ,n) and ^{10}B(γ, p) reactions and shell-model calculations.

*Current Address: Iwanuma City Office, Sakura, Iwanuma 989-2480, Japan.
†Current Address: Research Center for Nuclear Physics, Osaka University, Ibaraki 567-0047, Japan.
‡Current address: Department of Physics, Yamagata University, Kojirakawa, Yamagata 990-8560, Japan.
§Current address: Toshiba Corporation, Shinsugita, Isogo-ku, Yokohama 235-8532, Japan.
‖Current address: Graduate School of Engineering, Hokkaido University, Kita 13 Nishi 8, Sapporo 060-8628, Japan.
¶Current address: Rise Corporation, 3-9-15, Tsutsujigaoka, Miyagino-ku, Sendai 983-0852, Japan.

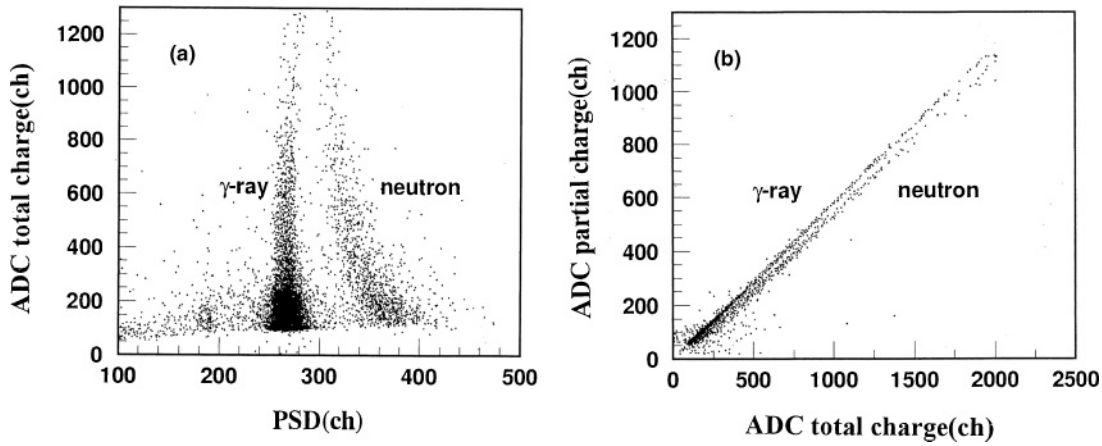

FIG. 1. n/γ discrimination by the (a) PSD module and (b) charge-comparison method.

II. EXPERIMENTAL PROCEDURE

The ^{10}B$(e,e'n)$ experiment was performed using the continuous electron beam from the stretcher-booster ring at Tohoku University. A ^{10}B-enriched target (96.5%) of 340 mg/cm^2 thickness in the form of a disk of compressed granular boron was bombarded with 200-MeV electrons. The beam current was 150–200 nA with an 80% duty factor. Scattered electrons were momentum analyzed at $\theta_e = 28^\circ$ (the lower limit of a scattering angle measured) by a magnetic spectrometer and detected using a vertical drift chamber and three layers of plastic scintillators. The spectrometer has a solid angle of 5 msr and a momentum resolution of 0.05% within the accepted momentum bite of 5.3%. Neutrons emitted from the target were measured using eight NE213 liquid scintillator detectors.

The detectors were placed in the electron scattering plane at $\theta_n = 58^\circ, 83^\circ, 108^\circ, 133^\circ, 158^\circ, 213^\circ, 238^\circ$, and 263° relative to the electron-beam direction. Each detector was placed 85 cm from the center of the scattering chamber, allowing the neutron energy to be determined by the time-of-flight method. The neutron detectors were shielded with lead, paraffin, and concrete, and lead collimators were placed in front of 4-cm-thick bismuth plates to absorb scattered electrons and soft γ rays from the target. The neutron detectors were calibrated using γ rays from ^{22}Na, ^{137}Cs, ^{60}Co, and ^{88}Y sources. The Compton edge of the ^{137}Cs γ ray was utilized to set the detection threshold. The neutron efficiency for the detectors was determined using a ^{252}Cf source and an analytical calculation code. The intrinsic resolution of the neutron detectors in the energy range of interest is about 2.5 MeV. The details of the electronics, data acquisition, and detection efficiency are described elsewhere [8,9].

To remove γ-ray events, pulse-shape discrimination (PSD) modules and the charge comparison method were used. Typical n/γ discriminated spectra are shown in Fig. 1.

III. RESULTS AND DISCUSSION

A. Missing energy spectrum

Data were taken for the excitation energy range 18–33 MeV. Figure 2 shows the missing energy spectrum for the ^{10}B$(e,e'n)$ reaction. Energies corresponding to transitions to the ground and excited states in ^{9}B are denoted by arrows. A peak at 8.4 MeV corresponds to the ground-state transition, which is weak at this angle. Two prominent peaks are seen at approximately 15 and 21 MeV. They correspond to the population of the 6.97 MeV $7/2^-$ and 11.70 MeV $7/2^- + 12.06$ MeV $3/2^-$ states in ^{9}B. These groups are identified as n_5 and $n_{6,7}$. Some counts below the region of the n_0 emission represent a background, but they are negligible compared to the counts in the regions of the n_5 and $n_{6,7}$ peaks.

B. Cross section and angular correlation

The cross-section magnitudes were determined by summing the yield within a range of ± 0.75 MeV for each missing energy peak. The background was subtracted by making use of the region in which true events do not contribute. The resultant differential cross sections for the $(e,e'n_0)$, $(e,e'n_5)$, $(e,e'n_{6,7})$, and $(e,e'n_{\text{total}})$ reactions were obtained.

The angular correlations for these decay channels and total were obtained from the differential cross sections and are shown in Figs. 3–6 with the best-fit curves of Legendre polynomials described below. The angular correlations for the $(e,e'n_0)$ reaction show a strong forward-backward asymmetry, suggesting interference from a transition with the opposite parity to $E1$. The angular correlations for $(e,e'n_{6,7})$ and $(e,e'n_5)$ are strikingly similar, which suggests that n_6 decay

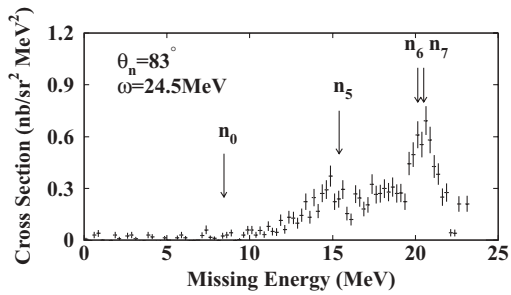

FIG. 2. Missing energy spectrum for the ^{10}B$(e,e'n)^9$B reaction at the excitation energy $\omega = 24.5$ MeV and $\theta_n = 83^\circ$.

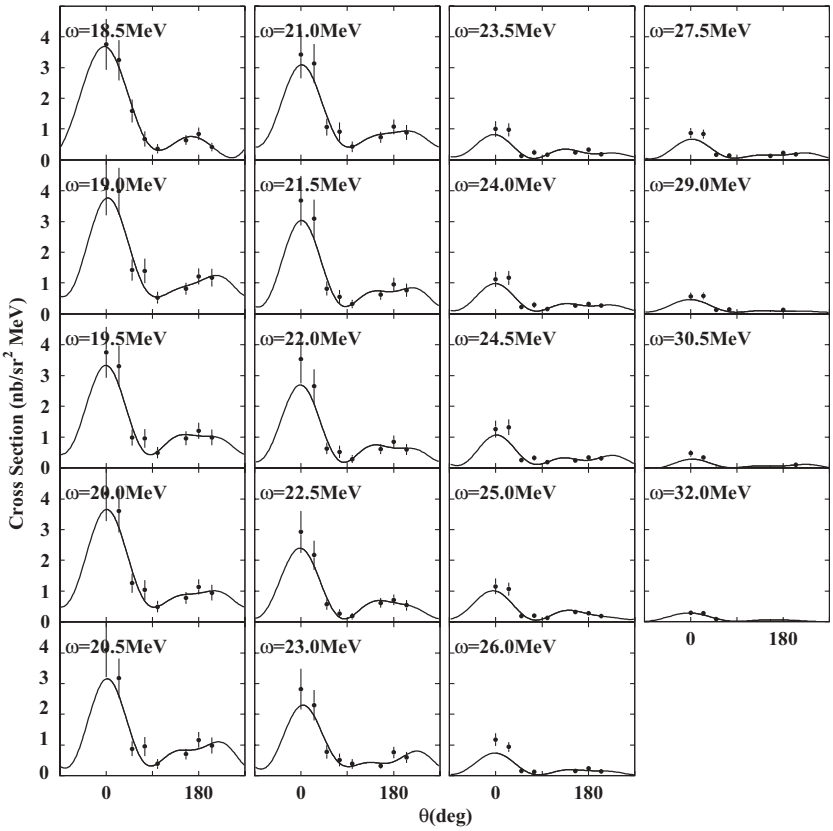

FIG. 3. Angular correlations for the n_0 neutron group. Solid curves are best fits of Legendre polynomials. Angles are relative to the momentum-transfer direction.

to the $7/2^-$ state is the main decay in the $(e,e'n_{6,7})$ reaction. A peak shift of about 50° for the forward peak is seen at lower excitation energy and returns to 0° above about 24 and 25 MeV for n_5 and $n_{6,7}$, respectively. The angular correlations for n_5 and $n_{6,7}$ are considerably different from those for n_0. These angular correlations were analyzed in the following way. The theoretical cross section can be written as [10,11]

$$d^3\sigma/d\Omega_e\, d\omega\, d\Omega_n = \sigma_M(V_L R_L + V_T R_T + V_{LT} R_{LT} \cos\phi_n + V_{TT} R_{TT} \cos 2\phi_n), \quad (1)$$

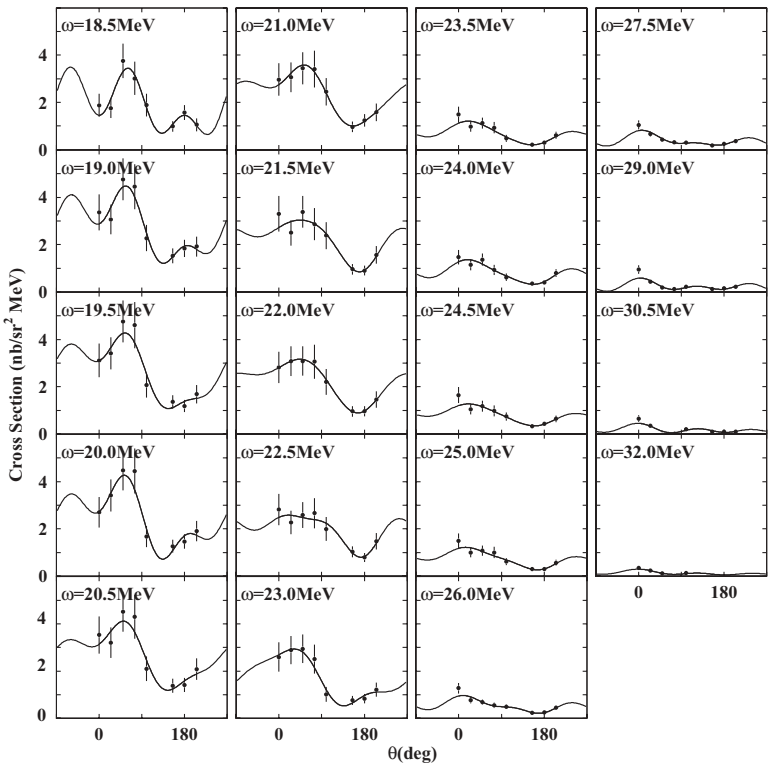

FIG. 4. Angular correlations for the n_5 neutron group. Solid curves are best fits of Legendre polynomials. Angles are relative to the momentum-transfer direction.

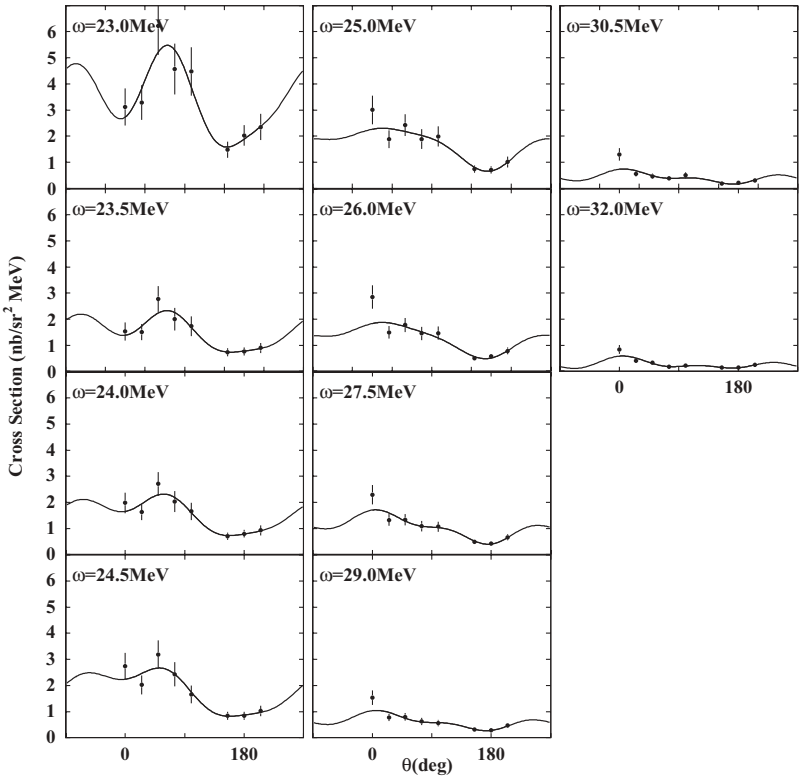

FIG. 5. Angular correlations for the $n_{6,7}$ neutron group. Solid curves are best fits of Legendre polynomials. Angles are relative to the momentum-transfer direction.

where σ_M is the Mott cross section for scattering on a point nucleus, and V_i are the leptonic kinematic factors. The response functions R_i contain all the nuclear structure information. Under the present experimental conditions, namely for forward scattering ($\theta_e = 28^\circ$) and low momentum transfer ($q_{\text{eff}} = 0.56$ fm^{-1}), the giant dipole resonance is excited predominantly via the longitudinal interaction ($C1$); the transverse component ($T1$) and other multipoles ($C2$) may

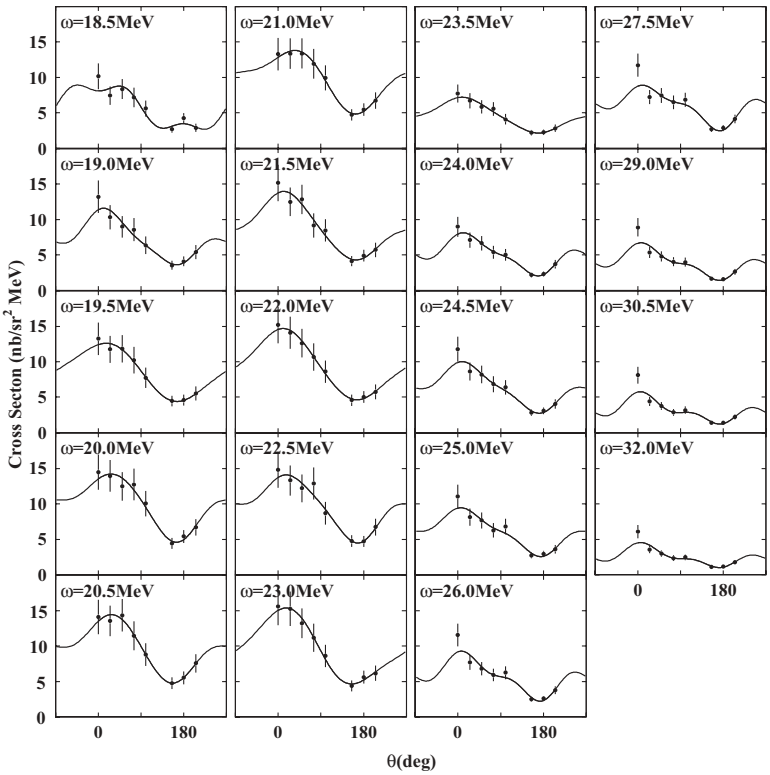

FIG. 6. Angular correlations for total neutrons. Solid curves are best fits of Legendre polynomials. Angles are relative to the momentum-transfer direction.

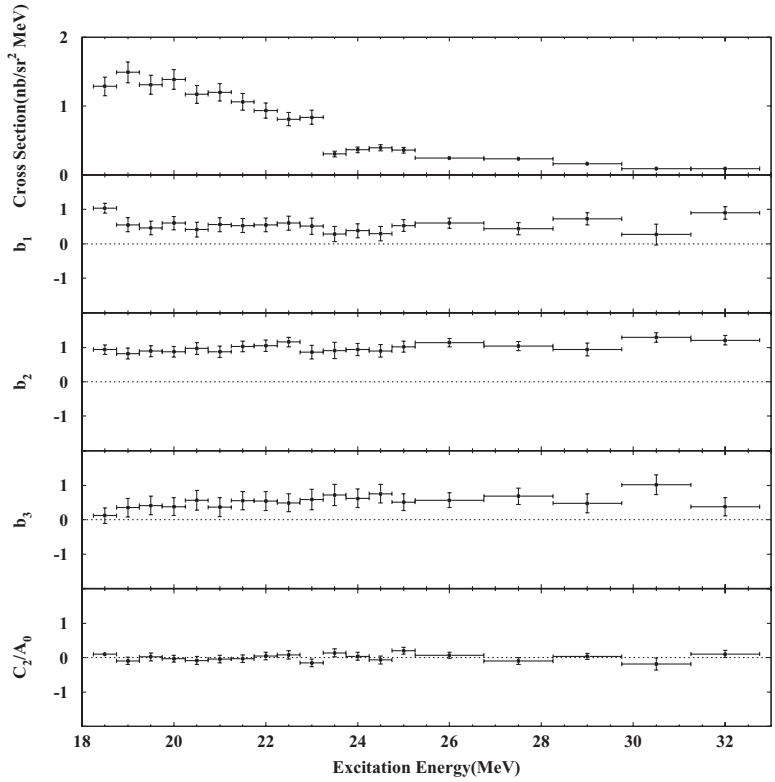

FIG. 7. Cross section ($4\pi A_0$) and angular coefficients b_i and C_2/A_0 for the n_0 neutron group.

be weakly excited. Under these conditions the longitudinal and transverse response functions, R_L and R_T, can be expressed by $|C1|^2$, $C1^*C2$, and $|T1|^2$. The interference terms R_{LT} can be expressed by $C1^*T1$ and $C2^*T1$, and R_{TT} by $|T1|^2$. The present response functions are approximated by a set of third-order Legendre polynomials and associated Legendre polynomials:

$$\begin{aligned} V_L R_L + V_T R_T &= A_0[1 + b_1 P_1(x_n) + b_2 P_2(x_n) + b_3 P_3(x_n)], \\ V_{LT} R_{LT} &= C_2\left[c_1 P_1^1(x_n) + P_2^1(x_n) + c_3 P_3^1(x_n)\right], \\ V_{TT} R_{TT} &= D_2 P_2^2(x_n), \\ x_n &= \cos\theta_n. \end{aligned} \tag{2}$$

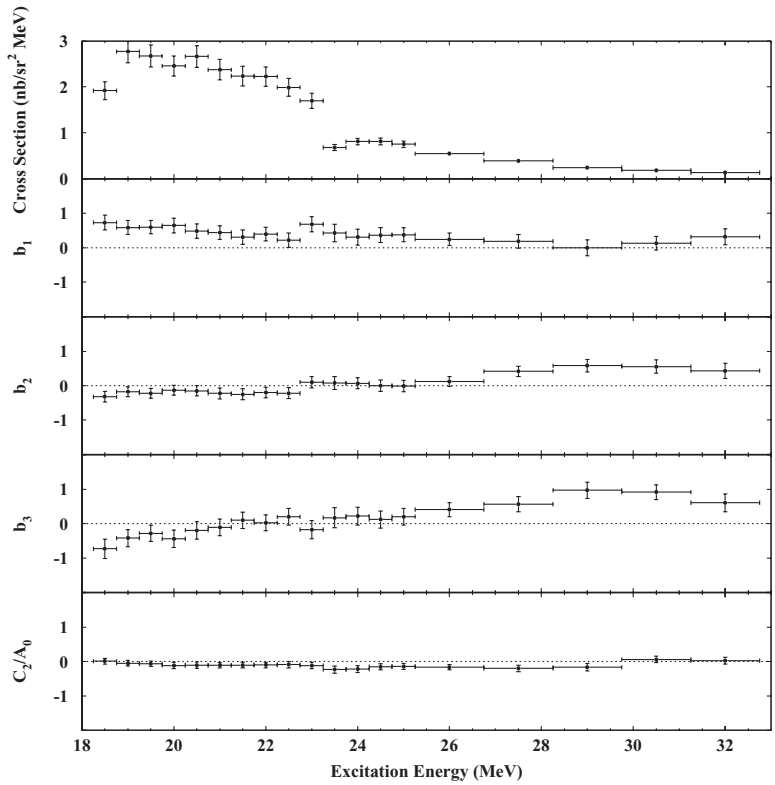

FIG. 8. Cross section ($4\pi A_0$) and angular coefficients b_i and C_2/A_0 for the n_5 neutron group.

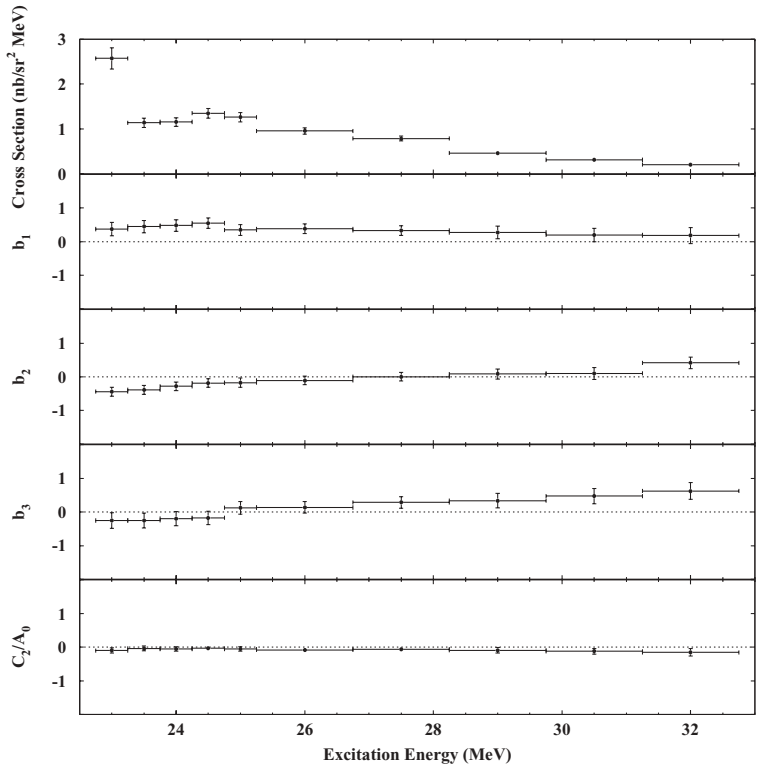

FIG. 9. Cross section ($4\pi A_0$) and angular coefficients b_i and C_2/A_0 for the $n_{6,7}$ neutron group.

In making a fit to the data, the following approximations were assumed. From the Goldhaber-Teller model [12], the ratio of transverse to longitudinal strength was estimated to be 2% at $E_x = 10$ MeV, increasing to 21% at $E_x = 30$ MeV. The transverse term was less than the $C1$ term; therefore, the c_1, c_3, and D_2 terms were neglected. Consequently, the cross section can be expressed by five terms:

$$d^3\sigma/d\Omega_e\, d\omega\, d\Omega_n = A_0\sigma_M\big[1 + b_1 P_1(x) + b_2 P_2(x) + b_3 P_3(x) - (C_2/A_0)P_2^1(x)\big], \qquad (3)$$

where A_0, b_1, b_2, b_3, and C_2 are fitting parameters.

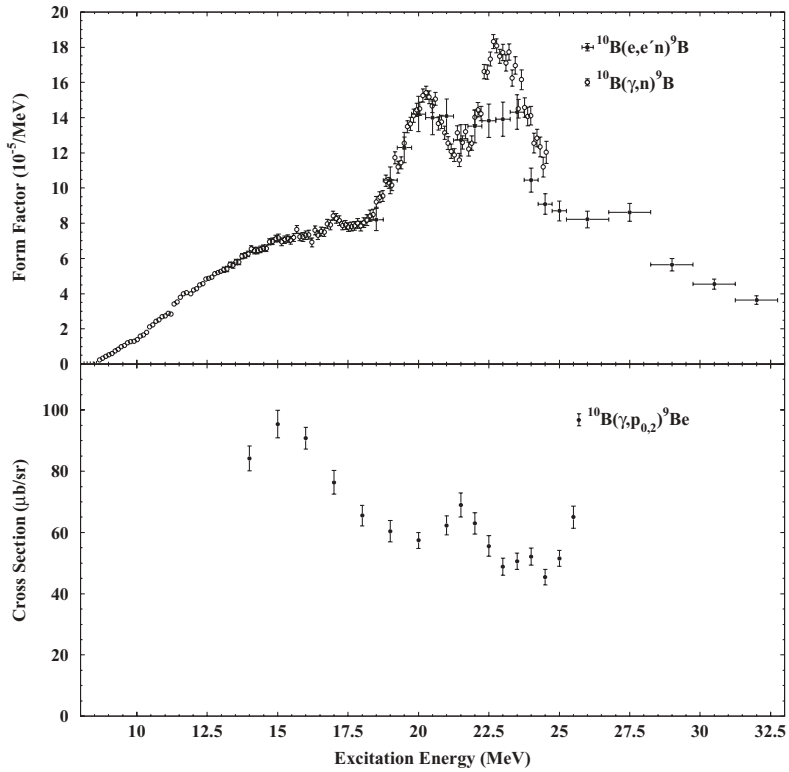

FIG. 10. Comparison of the cross sections. Upper panel: ^{10}B$(e,e'n)^9$B and ^{10}B$(\gamma,n)^9$B (Ref. [1]). Lower panel: ^{10}B$(\gamma,p_{0,2})^9$Be (Ref. [7]). The cross sections in the upper panel are transformed into the form factor.

The experimental angular correlations for each excitation energy region were fitted with Eq. (3), and the Legendre polynomial coefficients were obtained. The $4\pi A_0$, b_1, b_2, b_3, and C_2/A_0 parameters for the $(e,e'n_0)$, $(e,e'n_5)$, and $(e,e'n_{6,7})$ reactions and the $4\pi A_0$ parameter for the $(e,e'n)$ reaction were obtained on ^{10}B. The parameters $4\pi A_0$, b_1, b_2, b_3, and C_2/A_0 for n_0, n_5, and $n_{6,7}$ transitions are shown in Figs. 7–9, respectively.

A shift of the forward peak in the n_5 and $n_{6,7}$ transitions can usually be explained by interference between the longitudinal and transverse terms, namely C_2/A_0 [13]. However, C_2/A_0 values for the n_5 and $n_{6,7}$ transitions are negligible in the range measured, as shown in Figs. 8 and 9. The angular coefficient relates to the longitudinal matrix elements in the static limit of resonance approximation [10], assuming that only $C0$, $C1$, and $C2$ excitations contribute [14]. The angular coefficient b_i multiplied by A_0 is expressed as

$$\begin{aligned} A_0 &= C0^2 + C1^2 + C2^2, \\ A_0 b_1 &= 2\sqrt{3}\left[C0C1\cos\delta_{10} + \frac{2}{\sqrt{5}}C1C2\cos(\delta_{10}-\delta_{20})\right], \\ A_0 b_2 &= 2\left(C1^2 + \frac{5}{7}C2^2 + \sqrt{5}C0C2\cos\delta_{20}\right), \\ A_0 b_3 &= \frac{6}{5}\sqrt{15}C1C2\cos\delta_{21}, \\ A_0 b_4 &= \frac{18}{7}C2^2, \end{aligned} \tag{4}$$

where phase differences δ_{10} and δ_{20} are defined as $\delta_1 - \delta_0$ and $\delta_2 - \delta_0$, respectively. In the present analysis, the term b_4 is not included because b_4 contribution was negligible in an analysis including the term b_4. The change in the sign of b_2 and b_3 for the n_5 and $n_{6,7}$ decays (negative below and positive b_4 above ~24–25 MeV) can be supposed to depend on the signs of the phase differences $\cos\delta_{21}$ and $\cos\delta_{20}$ from Eq. (4).

C. Comparison with the photoreaction

The total cross section ($4\pi A_0$) for ^{10}B$(e,e'n)$ was obtained from an analysis of the angular correlation for the sum of n_0, n_5, and $n_{6,7}$ yields (Fig. 6). The cross section for the photoneutron reaction [1] has been transformed into the form factor by the usual method [15], which assumes that the photoneutron cross section is completely an $E1$ transition. Both cross sections transformed into the form factor are compared in the upper part of Fig. 10. The ^{10}B$(e,e'n)$ form factor agrees fairly well with the ^{10}B(γ,n) form factor except for a peak at about 23 MeV.

The ^{10}B$(\gamma,p_{0,2})$ cross section [7] is shown in the lower part of Fig. 10. The $(\gamma,p_{0,2})$ cross section is the sum of cross sections to the p_0 and p_2 transitions. A broad peak is indicated at about 15 MeV, which is larger than the region of the giant resonance at about 21 MeV seen in the $(e,e'n)$ reaction. The difference in binding energy between protons ($Q_m = -6.586$ MeV) and neutrons ($Q_m = -8.437$ MeV) seems not to influence the difference of the cross section. The small cross section at the peak of the giant resonance may reflect the lack of transition to high-lying states as observed in the $(e,e'n)$ reaction.

D. Comparison with shell-model calculations

The partial and total cross sections for the photodisintegration of the ^{10}B nucleus were calculated within the framework of the shell model with intermediate coupling by Gol'tsov and Goncharova [5]. In the calculations, the partial cross

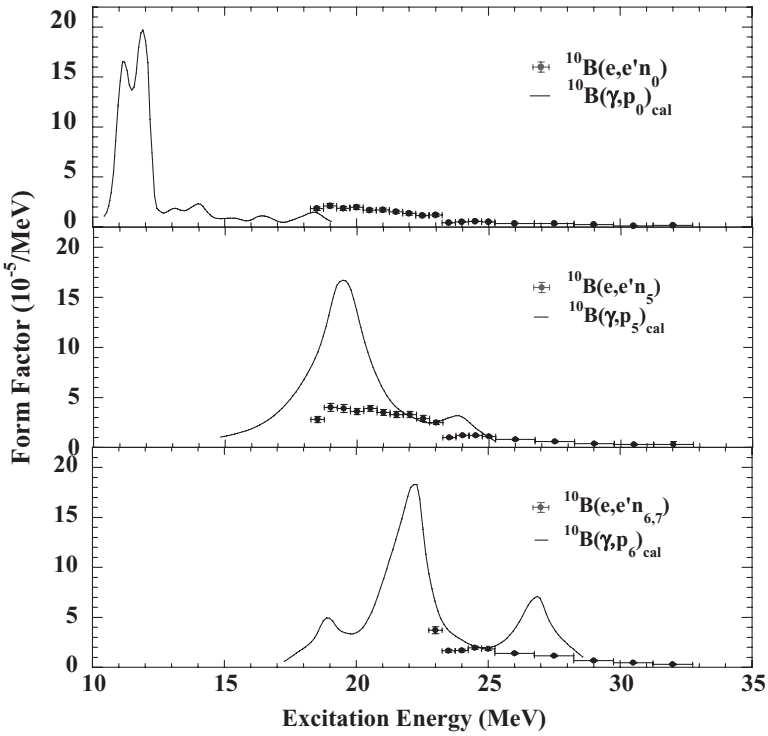

FIG. 11. Comparison of present results with the shell-model calculations from Ref. [5] for the n_0, n_5, and $n_{6,7}$ transitions. In the calculations, partial cross sections for photoproton and photoneutron channels are nearly the same.

sections for photoproton and photoneutron channels are nearly same. The present data for the n_0, n_5, and $n_{6,7}$ transitions are compared with the photoproton calculations in Fig. 11. In the experiment, the $(e,e'n_0)$ cross section was observed up to ~32 MeV beyond the predictions. For the n_5 transition, a pronounced peak in the cross section was not observed, but both cross sections agreed in the tail region. For the $n_{6,7}$ transition, two prominent calculated peaks were not observed in the measured range. It was confirmed that neutrons from the giant resonance in ^{10}B have decayed not only to the ground state but also to high-lying states in ^{9}B, although their cross sections are not as large as the predicted values.

IV. SUMMARY

The cross section and angular correlations to several residual states following the ^{10}B$(e,e'n)$ reaction were measured in the excitation energy region of about 18–33 MeV at an effective momentum transfer of 0.56 fm^{-1}. The populations to the ground (n_0), 6.97 MeV $7/2^-$ (n_5), and 11.70 MeV $7/2^- + 12.06$ MeV $3/2^-$ ($n_{6,7}$) states were observed. The cross sections for each transition were compared with shell-model calculations. The cross section for n_0 was measured up to 32 MeV, which is beyond the predictions. For the n_5 transition, a pronounced peak in the calculated cross section was not observed, but both cross sections agreed in the tail region. For the $n_{6,7}$ transition, two prominent peaks in calculations were not observed in the measured range. The angular distributions for n_0 show a strong forward-backward asymmetry, which suggests interference from a transition with parity opposite of $E1$. The angular distributions for n_5 and $n_{6,7}$ show a shift of about 50° for the forward peak. It might depend on the signs of the phase differences $\cos\delta_{21}$ and $\cos\delta_{20}$. The ^{10}B$(e,e'n)$ cross section was compared with the ^{10}B(γ,n) cross section; they agreed fairly well. It was confirmed that neutrons from the giant resonance in ^{10}B have decayed not only to the ground state but also to the 6.97 MeV $7/2^-$ and 11.70 MeV $7/2^- + 12.06$ MeV $3/2^-$ states in ^{9}B, although their cross sections are not as large as the predicted values.

[1] M. H. Ahsan, S. A. Siddiqui, and H. H. Thies, Nucl. Phys. **A469**, 381 (1987).
[2] E. Hayward and T. Stovall, Nucl. Phys. **69**, 241 (1965).
[3] R. J. Hughes and E. G. Muirhead, Nucl. Phys. **A215**, 147 (1973).
[4] U. Kneissl, K. H. Leister, H. O. Neidel, and A. Weller, Nucl. Phys. **A264**, 30 (1976).
[5] A. N. Gol'tsov and N. G. Goncharova, Sov. J. Nucl. Phys. **38**, 857 (1983).
[6] A. Kh. Shardanov and B. A. Yuryev, Yad. Fiz. **8**, 424 (1968).
[7] H. Ueno, H. Taneichi, Y. Takahashi, T. Suzuki, K. Shoda, T. Saito, and T. Tsukamoto, J. Phys. Soc. Jpn. **73**, 875 (2004).
[8] S. Suzuki, T. Saito, K. Takahisa, C. Takakuwa, T. Tohei, T. Nakagawa, Y. Kobayashi, and K. Abe, Nucl. Instrum. Methods **314**, 547 (1992).
[9] K. Kino, T. Saito, Y. Suga, M. Oikawa, T. Nakagawa, T. Tohei, K. Abe, and H. Ueno, Phys. Rev. C **65**, 024604 (2002).
[10] W. E. Kleppinger and J. D. Walecka, Ann. Phys. (NY) **146**, 349 (1983).
[11] G. Co' and S. Krewald, Nucl. Phys. **A433**, 392 (1985).
[12] M. Goldhaber and E. Teller, Phys. Rev. **74**, 1046 (1948).
[13] M. Cavinato, D. Drechsel, E. Fein, M. Marangoni, and A. M. Saruis, Nucl. Phys. **A444**, 13 (1985).
[14] M. Span, Th. Kihm, and K. T. Knöpfle, Z. Phys. A **330**, 345 (1988).
[15] C. Takakuwa, T. Saito, S. Suzuki, K. Takahisa, T. Tohei, T. Nakagawa, and K. Abe, Phys. Rev. C **50**, 845 (1994).